

**Spectropolarimetric Inversions of the Quiet Sun throughout
Solar Cycle 24**

by

James W. Crowley

Bachelor of Arts – Department of Astrophysical & Planetary Sciences

Undergraduate Honors Thesis

Defense Copy

Thesis Defense Committee:

Ivan Milic	Advisor	Department of Physics
Prof. Ann-Marie Madigan	Honors Council Representative	Department of APS
Prof. Adam Kowalski	External Faculty Member	Department of APS

To defend on:

March 31, 2022

This thesis entitled:
Spectropolarimetric Inversions of the Quiet Sun throughout Solar Cycle 24
written by James W. Crowley
has been approved for the Department of Astronomy and Planetary Sciences

Prof. Ivan Milic

Prof. Ann-Marie Madigan

Prof. Adam Kowalski

Date _____

The final copy of this thesis has been examined by the signatories, and we find that both the content and the form meet acceptable presentation standards of scholarly work in the above mentioned discipline.

Crowley, James W. (Bachelor's, Physics & Astronomy)

Spectropolarimetric Inversions of the Quiet Sun throughout Solar Cycle 24

Thesis directed by Prof. Ivan Milic

This project aims to study changes in the physical structure of the solar photosphere throughout solar cycle 24. To do this, we employ the use of two spectropolarimetric inversion codes combined with high spatial and spectral resolution observations from Hinode/SOT. The two inversion codes are a Milne-Eddington inversion code and a more complicated, depth-stratified code called SIR. By applying both inversion codes to the same datasets, we hope to determine whether models of different complexities are sufficient to find and characterize changes in concluded parameters. Notably, we focus on changes in the temperature structure and the line-of-sight velocity.

Contents

Chapter		
1	Introduction	1
2	Background	3
	2.1 Solar Structure & the Solar Cycle	3
	2.2 Radiative Transfer	4
	2.3 Milne-Eddington Model	6
	2.4 Local Thermodynamic Equilibrium (LTE)	8
	2.5 Spectropolarimetric Inversions	9
3	Data & Methods	11
	3.1 Datasets Selected	11
	3.2 Milne-Eddington Inversion Code	13
	3.3 SIR/DeSIRe	15
	3.4 Problems & Solutions with Inversions	15
4	Analysis	21
	4.1 Filtering & Clustering	21
	4.1.1 Filtering Pixels with Magnetic Field	22
	4.1.2 K-Means Clustering	23
	4.2 Comparing SIR Inversions to an Independent Inversion Results	25

5	Results	28
5.1	Temperature Gradient	28
5.2	Line-of-Sight Velocity	32
6	Conclusion	35
6.1	Future Work	36
	Bibliography	37

Figures

Figure

- | | | |
|-----|--|----|
| 2.1 | A diagram of how the solar dynamo explains the winding up of the toroidal fields of the active Sun, courtesy of Sanchez et al. [2014] | 4 |
| 2.2 | A small section of the solar spectrum, where different shaped lines are visible. The range of Hinode's spectropolarimeter is highlighted. | 9 |
| 3.1 | Example of a Hinode data; Left: continuum intensity observation of Stokes I, Right: observed normalized spectra of Stokes I for boxed pixel | 13 |
| 3.2 | An asymmetric line profile, unable to be well-fit by a Milne-Eddington atmosphere, which produces only symmetric inverted spectra. | 14 |
| 3.3 | Top: An example of a height stratified temperature, inverted via SIR. Bottom: the corresponding inverted spectra (solid), plotted on-top of the observed spectra (dotted). | 16 |
| 3.4 | Maps of inverted temperatures at $\log \tau = 0$ (right) and calculated χ^2 (left) for increasing rounds of median filtering. | 20 |
| 4.1 | The Stokes V spectra of the two boxed pixels. | 22 |
| 4.2 | Comparing the two methods of filtering magnetic fields: on the left is the polarization threshold method created for the ME model as a proxy for magnetic field strength; on the right is the directly inverted magnetic field from SIR. The color bars have been adjusted to show the similarity of features between the two. | 24 |

4.3	Comparing K-Means Clustering and LOS Velocities. K-Means clusters on the left; Inverted LOS velocities on the right. The structures and groupings are similar between both graphs.	25
4.4	Comparing the average temperature between inversion methods. Blue is SIR, yellow is NICOLE inversion of the same dataset.	26
5.1	Inverted Milne-Eddington Source Function Gradient, of all spectra. Dashed lines denote the mean values of the two distributions.	29
5.2	Inverted Milne-Eddington source function gradient, in granules (left), and intergranules (right)	30
5.3	Temperature gradient between different pairs of optical depths. From top to bottom, the graphs show temperature gradients between $\log(\tau) = 0$ and -1; 0 and -2; and -1 and -2, in granules (left) and intergranules (right).	31
5.4	Inverted Milne-Eddington Line-of-Sight velocities, in granules (left), and intergranules (right), in km/s.	32
5.5	Inverted Line-of-Sight velocities by SIR at optical depths of $\log(\tau) = 0$, -1, and -2 in intergranules (left) and granules (right), in km/s.	34

Chapter 1

Introduction

Because of its proximity, high spatial, spectral and temporal resolution observations of the Sun allow us allow us to ask and answer fundamental questions, as well as understand and test cutting-edge models of the Sun and other stars. One of the most important ways this is achievable is through studying the solar spectrum; because the solar spectrum is formed by light propagating through the solar atmosphere, inherently embedded in the spectrum is the information about the physical structure and properties of the Sun. By observing spectral lines and modeling the processes that form and change the shape of the spectral lines, it's possible to diagnose physical properties of the solar atmosphere. By combining models of the solar atmosphere and the atomic data that describes absorption / emission processes, it is possible to create so called spectropolarimetric inversion codes. These are computer programs that find the model atmosphere which best fits the observed (generally polarized) spectrum. This allows us to interpret high resolution spectropolarimetric observations and, ultimately, map the solar atmosphere in all three dimensions.

An important and well known property of the Sun is the 11-year solar magnetic cycle - first observed in 1843 by H. Schwabe, the 11-year solar cycle manifests itself through the number of sunspots, magnetic activity, and solar radiation. Despite being well documented and studied, predicting in detail the solar cycle, flares, and magnetic activity remains one of the most important pursuits in solar physics. There's about as many ways to study the solar cycle as there are to observe the Sun - from Wolf's original and simple method of counting sunspot numbers [see e.g. Clette et al., 2014], to using the polarization of the light to infer the structure of the magnetic field

[e.g. using inversions, see del Toro Iniesta and Ruiz Cobo, 2016], there are various ways to study the changing structure of the Sun throughout the magnetic cycle. Understanding and predicting changes in the magnetic structure of the Sun is hugely important and one of the biggest open questions in solar physics.

In this project, we look for the systematic changes in the physical structure of the solar atmosphere throughout solar cycle. To do this, we use high spatial and spectral resolution spectropolarimetric observations of the solar atmosphere, made by the spectropolarimeter onboard Hinode/SOT solar telescope [Lites et al., 2013]. We focus on the parts of the atmosphere that exhibit no detectable magnetism and apply multiple inversion codes to the spectropolarimetric observations. We are mostly interested in the thermodynamic structure, namely the temperature gradient and the line-of-sight velocity. We discuss the results obtained by the different inversion approaches but also try to determine whether the resolution of the Hinode and the complexity of the chosen inversion codes are sufficient to detect and diagnose changes in the solar photosphere throughout the solar magnetic cycle.

Chapter 2

Background

2.1 Solar Structure & the Solar Cycle

The Sun is a very complicated object, largely due to the wide magnitude of physical parameters and processes taking place across the radius of the Sun. Investigating the structure of the Sun requires the application of various methods of observation and modeling. For this reason, studies of the physical structure of the Sun typically restrict themselves to a specific range of radii, temperatures, or specific physical processes, which are pieces of a larger picture of the structure of the Sun.

A property central to the Sun is the Solar Magnetic Cycle: over a roughly 22 year period (two 11-year cycles of maxima and minima), the Sun's field flips twice back to its original orientation. This process is explained and modeled via the so-called solar dynamo [e.g. Charbonneau, 2010], the model of how the Sun generates its tangled and complicated magnetic field. In this model, a combination of differential rotation speeds (both with depth and latitude) on the Sun and the processes of charged plasma which make up the Sun cause a winding-up and periodic reversal of the Sun's magnetic dipole. During this process, however, the Sun's magnetic field becomes tangled, causing regions of large magnetic flux resulting from the field lines passing through the Sun's atmosphere.

Throughout the solar magnetic cycle, the tangled magnetic field causes small-scale events like flares and active regions. Even though large scale changes in the magnetic field are well understood through the model of the solar dynamo, details and small scale events are still unpredictable,

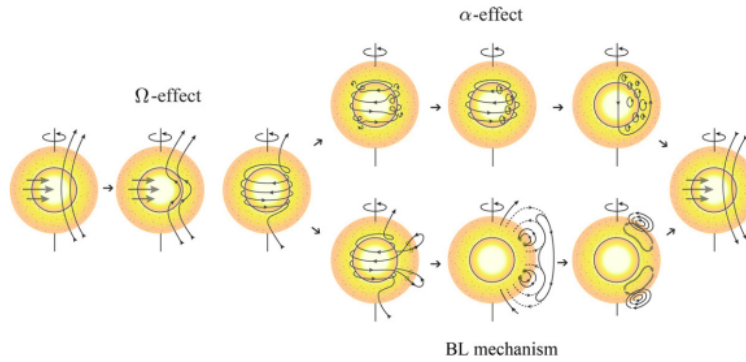


Figure 2.1: A diagram of how the solar dynamo explains the winding up of the toroidal fields of the active Sun, courtesy of Sanchez et al. [2014]

meaning a more complete picture of the Sun throughout the solar cycle is still an important inquiry in solar physics. This is a hugely important issue because flares, coronal mass ejections (CMEs), and other magnetic events can have measurable and significant effects on Earth, like disrupting satellites and electronics. Being able to predict and understand the structure of the Sun throughout the solar cycle is important not just for solar physics but many other branches of science.

In this project, we focus on the physical structure of the Sun's photosphere; the photosphere is the layer of the Sun's atmosphere where the density of particles drops enough so that it becomes transparent to photons across most wavelengths, allowing them to escape into space with little interaction. Therefore, this is what is typically meant by the "surface" of the Sun, and is a fascinating layer where the negative gradient of density, temperature, and opacity give rise to the formation of spectral lines. As these properties change with depth and the resulting opacity decreases, the formed spectral lines reflect the physical condition of the photosphere. By studying the shape of these lines, like ones seen in Fig. 2.2, it allows us to study the structure of the solar photosphere.

2.2 Radiative Transfer

Radiative transfer is the theoretical framework through which we can determine how light is modified as it passes through a material. The centerpiece of it is the equation of radiative transfer,

which is a mathematical formalization which says the elementary change in the intensity of the light that enters into that material depends on the absorption, emission, and scattering in the material.

In its full form, the equation of radiative transfer reads:

$$\frac{1}{c} \frac{\partial}{\partial t} I_\lambda + \hat{\Omega} \cdot \nabla I_\lambda + (k_{\lambda,s} + k_{\lambda,\alpha}) \rho I_\lambda = j_\lambda \rho + \frac{1}{4\pi} k_{\lambda,s} \rho \int_{\Omega} I_\lambda \Omega. \quad (2.1)$$

Where I is the incoming intensity into a layer of material, the j term describes the emission, and k describes the scattering, [Chandrasekhar, 1960]. It's common to rewrite the equation of radiative transfer in terms of the source function $S_\lambda \equiv \frac{j_\lambda}{k_\lambda}$, and the optical depth, τ_λ :

$$\frac{dI_\lambda}{d\tau_\lambda} = I_\lambda - S_\lambda. \quad (2.2)$$

with the so-called formal solution that reads:

$$I_\lambda = I_\lambda e^{-\tau_\lambda} + \int_0^{\tau_\lambda} S(t) e^{-t} dt. \quad (2.3)$$

Here the optical depth τ_λ is defined as:

$$d\tau_\lambda = -k_\lambda dz. \quad (2.4)$$

Here k_λ is the total absorption coefficient (opacity) at the wavelength λ , given in units of m^{-1} . The optical depth or optical thickness is a unitless ratio of distance over the length scale where $\frac{1}{e}$ of propagating light of a given wavelength is absorbed. This lengthscale is commonly known as the ‘‘mean free path.’’ The optical depth is dependent on the wavelength of light, as well as the properties of the material. It's a useful way of redefining physical depth in an atmosphere because it allows the RTE to be written in a way that is computationally easier to solve, at the loss of information about physical depth in the photosphere. The radiative transfer equation is relatively straightforward to solve if opacities and emissivities are explicitly known everywhere in the atmosphere and at all wavelengths of interest. To calculate opacities and emissivities, however, we must involve all the relevant physical processes that result in an absorption, emission or scattering

of a photon. For spectral line formation the most important is the absorption of a photon due to the excitation from a lower to an upper energy level of an atom. This process is known as spectral line absorption. The inverse process, emission of an excited atom is the spectral line emission. These processes give rise to the spectral lines in the spectrum of the Sun, but to properly model the solar radiation we also have to take into account various continuum processes: electron scattering, photoionization, three body processes, etc. In modern spectrum modeling codes, there are numerous processes taken into account and calculated by the so called “opacity packages.” To summarize, to solve radiative transfer equation for a set of wavelengths that describe our spectral line, we have to go through a substantial calculational effort of computing all the necessary opacity and emissivity processes and then integrating the equation of radiative transfer, that is, Eq. 2.3.

2.3 Milne-Eddington Model

The Milne-Eddington Model is a widely-used and important simplification of the atmospheric structure, and one that has been commonly used for the solar photosphere. Up until the past few decades, limitations on computationally intensive solutions to the RTE restricted solving the RTE to simpler models - the Milne-Eddington model is probably the most important of these. However, it is still relevant when it comes to the interpretation of the data or fitting the observed spectropolarimetric data by a model [Orozco Suárez et al., 2010, Borrero et al., 2011].

In the Milne-Eddington (ME) atmosphere, all physical conditions of the atmosphere are constant throughout the considered layer (usually photosphere), except the source function, which is changing linearly with continuum optical depth. The parameters of this model are derived from the processes which form and shape spectral lines. However they’re not always directly relatable to physical quantities like temperature, pressure, and abundances.

In the Milne-Eddington model, a spectral line is parameterized by 6 variables, which describe the shape of the line profile and the source function behavior. These variables are derived from spectral line formation and broadening processes. The simplicity and broad-scope of the model means that, even though it’s fast to solve and widely applicable, it has some inherent problems and

uncertainties, which will also be discussed below. The shape of the spectral line is described by the line absorption profile, ϕ_λ , that is taken to be constant with depth. The absorption profile is the convolution of a Gaussian and a Lorentzian profiles and is called a Voigt profile; The Gaussian part comes from the random motion of particles in the photosphere, causing Doppler shift, and the Lorentzian part comes from natural and pressure broadening of atomic energy levels [see, e.g. Collins, 1989]. Together, the two processes result in a profile which has characteristics from each constituent part. The line absorption profile is proportional to the probability distribution of the absorption of light in the given spectral line over the wavelength. It relates wavelength-dependent optical depth to the continuum optical depth in a very simple way:

$$\tau_\lambda = \eta\tau \phi_\lambda(v_{\text{los}}, \Delta v, a). \quad (2.5)$$

The line absorption profile is therefore described by three parameters that characterize the shape of the Voigt function:

- v_{los} refers to the line-of-sight Doppler velocity, and in the Milne-Eddington model, this uniquely describes the shift of the line from the central, "rest" wavelength of the spectral line.
- Δv is the micro-turbulent Doppler velocity, characterizes the amount spectral line broadening due to the unresolved Doppler shifts
- a is referred to as the "line damping", which describes the processes which broaden the energy levels of individual particles. This broadens the line profile in a different way than Δv , and largely effects the wings of the spectral line. In the photosphere it mostly depends on the gas pressure.

The parameter η is the line strength, defined as the ratio between the opacity due to spectral line processes, at the line center and the continuum absorption. This value depends the amount of absorbers that the propagating light encounters, and therefore describes the strength or depth of the spectral line.

If we assume the constant line absorption profile and the linear behavior of the source function, $S = a_0 + a_1\tau$, Eq. 2.3 yields:

$$I_\lambda = a_0 + \frac{a_1}{1 + \eta\phi_\lambda}. \quad (2.6)$$

This is a very simple equation that can be used to intuitively understand behavior of solar spectral lines (e.g. lines formed in the region of higher source function gradient are deeper), but is especially convenient for devising simple diagnostics method, i.e. spectroscopic or spectropolarimetric inversions.

2.4 Local Thermodynamic Equilibrium (LTE)

In more general approaches, opacity and emissivity are allowed to vary with depth in the atmosphere, and are derived from the physical parameters: temperature, velocity, pressure, etc, that are also depth-dependent. In the photosphere, it is common to assume that the so called local thermodynamic equilibrium (LTE) approximation holds. In order for LTE to hold, photons and particles need to be in thermal equilibrium, which allows us to make assumptions about distributions of particles. For instance, Maxwellian distribution of particle velocities, Saha distribution for ionization, and Boltzmann distribution for excitation. Despite these simplifications, solving the full radiative transfer problem is still computationally difficult and requires computer codes to solve efficiently. In order to solve the equation of radiative transfer, we need the coefficients of absorption and emission, which depend on the physical condition of the solar atmosphere, and vary with height and wavelength. Once coefficients of absorption and emission (opacity and emissivity) are known, solving the RTE yields the outgoing spectra of the Sun. This is the so-called forward problem. Going the other direction by using the observed spectra to deduce physical conditions of the Sun is the so-called inverse problem, which is even more computationally intensive, and is the goal of spectropolarimetric inversions (in short - inversions).

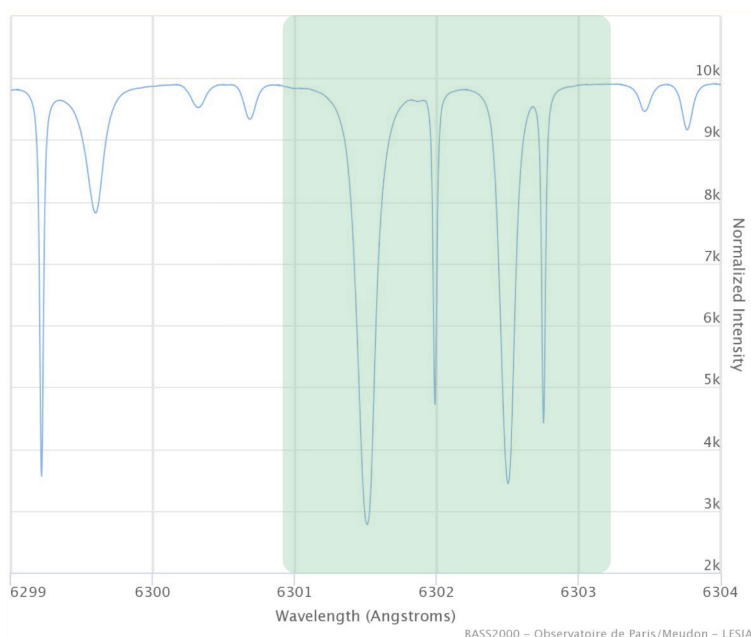


Figure 2.2: A small section of the solar spectrum, where different shaped lines are visible. The range of Hinode's spectropolarimeter is highlighted.

2.5 Spectropolarimetric Inversions

Inversion codes are schemes which combine models of stellar atmospheres, atomic physics and RTE solvers with a merit-function optimizer in order to determine the model parameters which best reproduce the observable (in this case, polarized spectra). They're best understood through contrast to synthesis codes. Synthesis codes are found across all branches of science: they're a model of an observable phenomena where the variables or parameters of the model are used by some relation or equation to predict what one would observe. In the context of solar spectropolarimetry, this means using model parameters which correspond to physical conditions of the solar atmosphere, like temperature, pressure, atomic abundances, and so on, in order to predict what emergent spectra would be observed. With this picture in mind, it's easier to understand what is meant by an inversion code: it works in exactly the opposite direction. Using a observed solar spectra, it finds the combination of physical parameters which would best reproduce the measured spectra.

This means there's a couple things required for a working inversion code: first is a model of

how the physical conditions of the solar photosphere work together to produce spectra, and how changes in these conditions will change the observables [so called response functions, Ruiz Cobo and del Toro Iniesta, 1992]. The next is an optimizer, which is able to quickly and efficiently find the combination of parameters which best reproduce the observable. This is done by defining a merit function, which mathematically evaluates how closely a model spectra resembles the observed one, and combining it with a method to step through parameter-space to find the combination of parameters which minimizes the merit-function.

Although the process sounds straightforward, in practice, there's countless different ways to carry about inversions, each with unique advantages and disadvantages. Fundamentally, differences in inversion methods come from the fact that completely simulating all possible physics occurring in the solar photosphere is impossible, and simplifications and assumptions are required. Some of these might include differences in equations of state, the height dependence of different physical parameters, or different methods to numerically solve the equation of radiative transfer.

For this project, two inversion codes were used. One is a code using a Milne-Eddington approximation, designed for this project, which fits the Eq. 2.6 to the observed intensity spectrum. The more complicated (and realistic) scheme is the code called SIR, designed and written by Ruiz Cobo and del Toro Iniesta [1992]. Contrary to the Milne-Eddington approximation, SIR allows for depth-dependent temperature, velocity, pressure and the magnetic field. It iteratively modifies the starting atmosphere until a good fit to the observed spectrum is found. By applying these codes to the maps of the polarized spectra observed by the Hinode/SOT SP instrument, the inversion schemes provide maps of the inverted parameters that describe the solar atmosphere. In the case of the Milne-Eddington inversion, these are maps of the parameters that appear in the Eq. 2.6, while in the case of SIR, these are the maps of the temperature and velocity at different depths in the solar atmosphere.

Chapter 3

Data & Methods

3.1 Datasets Selected

In order to characterize and study the quiet (i.e. non magnetic) solar photosphere throughout the solar cycle, a specific data is needed: as detailed above, we know from our models and laboratory studies of atomic energy levels that different atomic transitions occur under different physical conditions. To study the solar photosphere, a well understood transition (that is, spectral line) "formed" in the photosphere is required. Next, we need consistent data from throughout the solar cycle, which allows for the study of temporal changes in the photosphere. Additionally, two more requirements are necessary for our study of the quiet Sun in particular. First, it's important that this line is observed with high spectral resolution: the higher spectral resolution we have, the more detail we have about the shape of the line, allowing inversions with less uncertainty. The other requirement revolves around the concept of **unresolved magnetic flux**. It has been shown that magnetic flux in the photosphere modifies spectral line profiles by changing temperature, intensity, and other quantities [Criscuoli et al., 2013]. In the context of the quiet Sun, unresolved magnetic flux refers to the effect when differently-oriented magnetic fields or fields of varying strength in a single spatial bin (pixel) average together to cause the polarization of the pixel to appear non-magnetic, when the magnetic flux on scales smaller than resolvable is, in fact, modifying the spectral line. To minimize the effect of unavoidable unresolved magnetic flux, another requirement is imposed on the selection of data: we require high spatial resolution. This is because, in order to characterize non-magnetic regions of the Sun's surface, it's critical to be able to identify and

set aside pixels containing small-scale magnetic elements, and higher spatial resolution limits the amount of possible unresolved magnetic flux.

For these reasons, datasets observed by the Hinode/SOT SP instrument [Lites et al., 2013] from throughout the solar cycle were selected. The high spectral (approximately 0.002 nm) and spatial (0.3 arcseconds, that corresponds to roughly 200 km on the solar surface) resolution of Hinode spectropolarimeter make it a perfect candidate for this project. Hinode observes two Fe I absorption lines formed in the solar photosphere, at 630.15 nm and 630.25 nm. These lines have different magnetic sensitivities of $g_{630.15nm} = 1.67$ and $g_{630.25nm} = 2.50$. For this project, the 630.15 nm line was chosen because of its lower magnetic sensitivity. This means that any variations in the inferred parameters are less likely to be due to magnetic interactions. Additionally, by focusing on a single line, we eliminate the systematic uncertainty that comes from inverting two lines simultaneously. When we fit two lines, the noise and errors from both lines influence the inverted parameters. By focusing on the 630.15 nm line, we focus on non-magnetic influences on the line shape, as well as reduce systematic uncertainty. Hinode SOT/SP observes the intensity and the polarization of the light at 112 wavelength points, with spectral sampling of 0.00215 nm. This leads to datasets of four-dimensional data, where at each (x, y) spatial point has 112 wavelength points for each of the 4 Stokes components. However, for this project, since it focuses on the spectral line at 630.15 nm, only the first 60 wavelength components were considered. We also took polarization of the light into account when inverting the data, but we use the inferred magnetic field only to filter out unwanted (i.e. magnetic) pixels.

Datasets were selected from the High Altitude Observatory's Community Spectropolarimetric Analysis Center (CSAC) data archive. CSAC houses publicly available calibrated Hinode data from throughout the satellite's mission. From CSAC's Hinode archives, a few datasets were stringently selected - in addition to the requirements listed above, a few more were applied. First, datasets were selected to be without sunspots and active regions; Secondly, only the datasets near the disk center were selected (heliocentric radial angle $\mu \geq 0.90$). This was done to keep inversions as simple as possible and not introduce any projection effects.

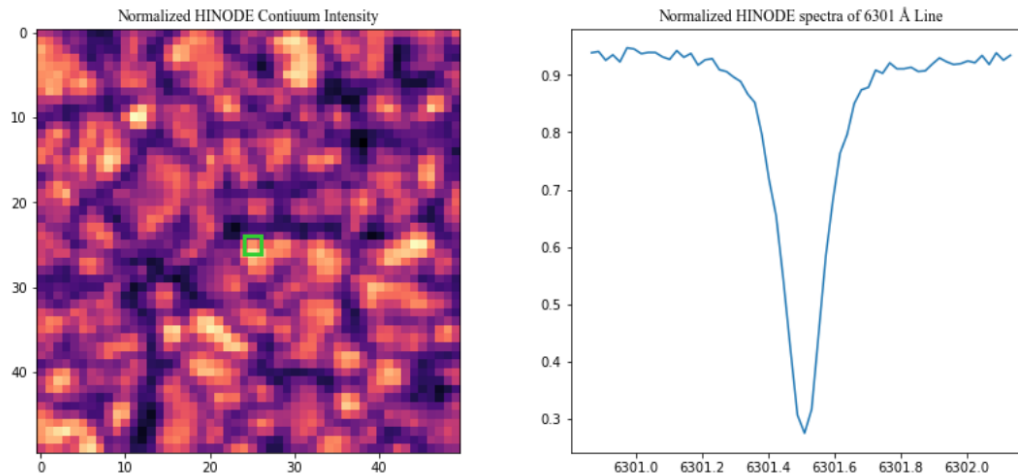


Figure 3.1: Example of a Hinode data; Left: continuum intensity observation of Stokes I, Right: observed normalized spectra of Stokes I for boxed pixel

With these criteria in mind we selected total of three datasets from throughout solar cycle 24. The first was chosen for its proximity to the solar minima, and was observed on 2008-12-18 around 03:06. Likewise, the second was chosen with the above criteria in mind and to be near the solar maxima; it was observed on 2014-06-05, around 22:00. Additionally, one more dataset was used in this project; this was included as part of the verification of results and analysis. This dataset was observed by Hinode on 9-24-2007 at 19:32:10. It was selected because it was independently inverted by H. Socas-Navarro in 2011, [Socas-Navarro, 2011], using an inversion code named called NICOLE [Socas-Navarro et al., 2015].

3.2 Milne-Eddington Inversion Code

For this project, a Milne Eddington Inversion code was written in Python programming language. By applying the Milne-Eddington approximation outlined above (2.6) to the parameters of the Fe I line at 630.15 nm and defining the merit function as the so called χ^2 between the observed and the calculated spectrum, we created an inversion code by using an optimizer from the SciPy

Python package, to find the best combination of parameters in each pixel. Here, χ^2 is defined as:

$$\chi^2 = \frac{1}{60} \sum_i \left(\frac{I^{\text{obs}} - I^{\text{calc}}}{\sigma} \right)^2. \quad (3.1)$$

Here I^{obs} , I^{calc} and σ denote observed intensity, calculated intensity and the noise (uncertainty) of the observations, respectively, while the division with 60 represents averaging over all the considered wavelengths.

Because the ME model uses constant values of parameters throughout the photosphere for each pixel, it finds a single (average) value for every inverted quantity. This simple model is computationally easy to run, but any information about depth-dependency is lost. One such effect is in the Doppler shift of each pixel; without a varying LOS velocity, there is no way to explain asymmetric lines, like the one in the figure below. In the figure, the ME model has done its best to find parameters which reproduce the observed profile, but it has no way to account for asymmetric lines.

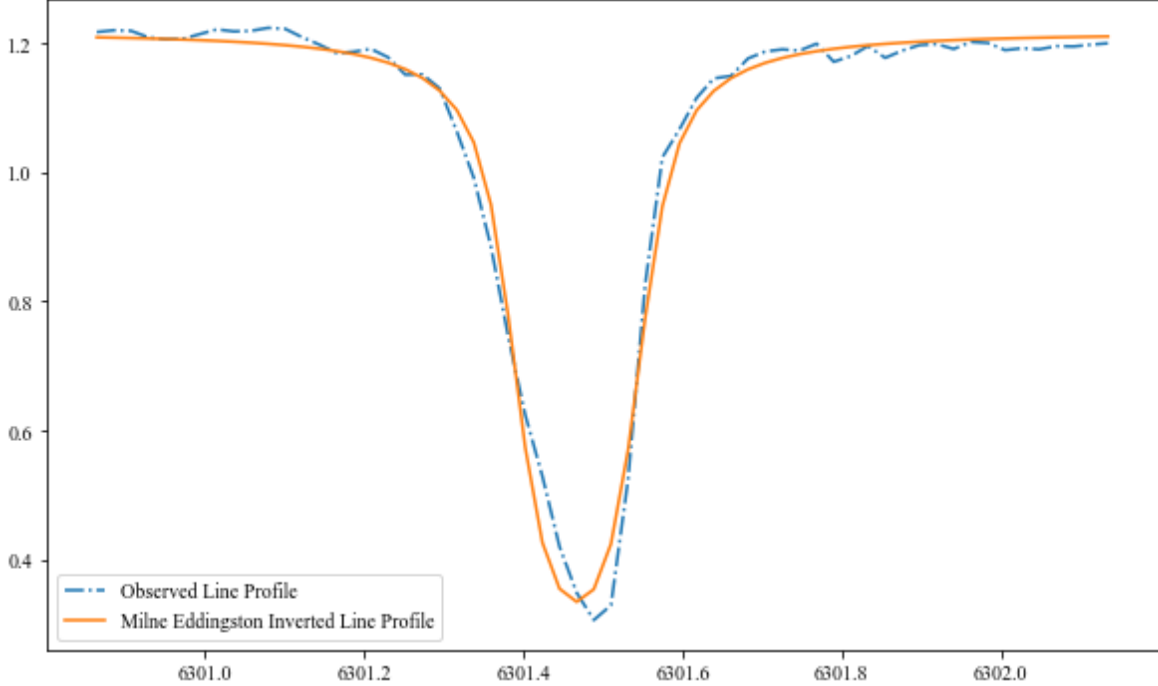


Figure 3.2: An asymmetric line profile, unable to be well-fit by a Milne-Eddington atmosphere, which produces only symmetric inverted spectra.

Luckily, in the datasets inverted for this project, most observed spectral lines are well approximated by a symmetric line profile. Additionally, asymmetric line profiles only make a large difference in quality of inversions (an increase in χ^2 greater than 10%) in approximately 5% of pixels. However, it's still a disadvantage of the ME atmosphere, which is important to consider.

3.3 SIR/DeSIRe

In 1992, solar physicists B. Ruiz Cobo and J. C. del Toro Iniesta developed a new code to invert the radiative transfer equation, which allows for the inversion of height-stratified quantities such as the temperature, magnetic field vector, and line-of-sight velocity [Ruiz Cobo and del Toro Iniesta, 1992]. This scheme has remained one of the most popular and applicable to the solar photosphere, and it has been updated and improved with new physics since its creation. It's named SIR, which stands for Stokes Inversions based on Response Functions. The power of SIR over a Milne-Eddington inversion is a more complicated model of the solar photosphere, which allows the code to invert physical parameters as a function of continuum optical depth, not just as a single value. An example of this for the temperature of an inverted spectra is shown below in Fig. 3.3. Recently, a team of researchers have created a python wrapper for SIR, which allows the inversion of many spectra in a field-of-view from a easier-to-use python script, which then runs the original SIR code in the background [Gafeira et al., 2021]. This python wrapper is the inversion code that was used for this project, and all the datasets were inverted both using Milne-Eddington code and SIR.

3.4 Problems & Solutions with Inversions

Despite the methods to carefully perform and optimize the inversions, they occasionally fail to find a satisfactory fit. When this happens, additional steps are required to ensure the quality of inverted parameters. When an inversion does "fail," this usually takes one of two forms:

- the code "can not converge" on a solution to the inversion, or;

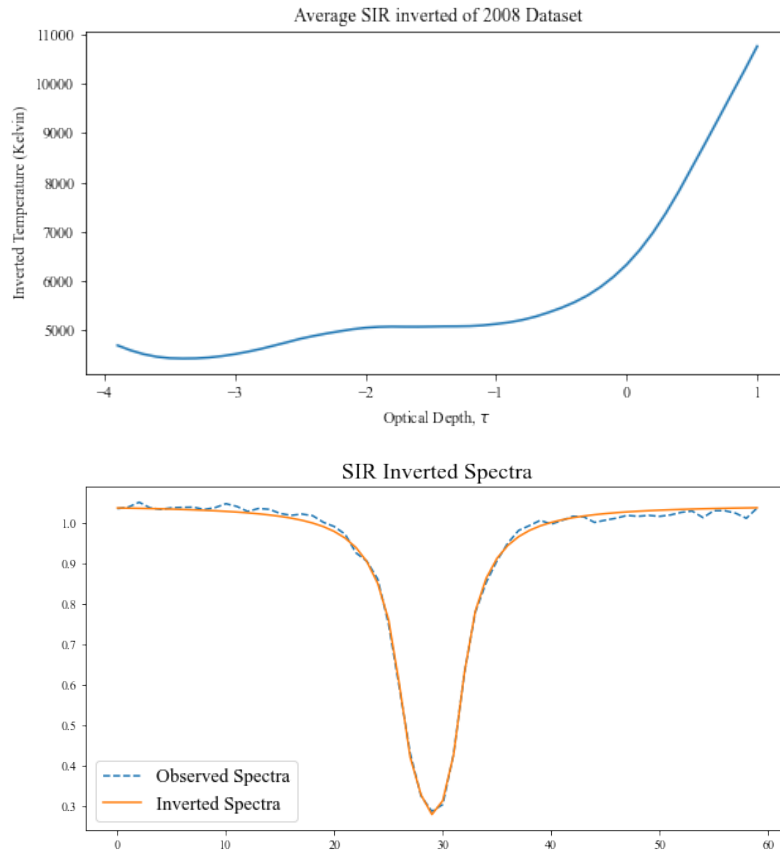


Figure 3.3: Top: An example of a height stratified temperature, inverted via SIR. Bottom: the corresponding inverted spectra (solid), plotted on-top of the observed spectra (dotted).

- the concluded parameters don't resemble physically realistic or expected values.

The first can occur for a variety of reasons, usually on the end of the optimizer - maybe the code's optimizer hits a maximum number of of allocated steps to get to the best solution, or a starting parameter set is so far from the best solution that the optimizer doesn't know which way to step in parameter-space to get closer. Solutions to inversions failing to converge involve many different methods, but the most effective solution is to provide the code with an initial solution as close to the best fitting ones as possible. Other solutions implemented in this project for the problem of inversions failing to converge include allocating more steps and more time for the code to run, or re-inverting non-converged spectra using a different optimizer or different step sizes through

parameter space.

The second problem is much more complicated and harder to solve. It stems from a more fundamental issue with all inversions, regardless of method or model - it goes by a few names, but they all refer to the same issue: non-orthogonal parameters, degenerate solutions, or non-injective mapping of solutions. This means that different combinations of model parameters can produce identical or nearly identical solutions (here, solutions are inverted line profiles). This problem is exacerbated by the fact that noise in the observed data, both random and systematic, can slightly change the observed line profile, which can have huge changes on inverted parameters. These separate issues both produce a similar outcome for inversion: inverted parameters that don't resemble physically realistic or expected conditions on the Sun. By "expected" we mean: two very similar spectra result in two very different atmospheric models. There are few reasons for the existence of the degenerate solutions, but even after removing the observed noise and systematic errors, one persists: radiative transfer is a non-local process and different depth stratifications can produce identical spectra.

This issue can be thought of mathematically: the complicated solar model results in many local-minima in the χ^2 hypersurface, as well as many of the resulting local-minima being equally or nearly equally as good. This means that minimizing techniques, which often work by "stepping" through parameter space on the χ^2 hypersurface in order to find the minima in χ^2 , often get stuck or can not differentiate between different local minima. For this problem, a few different solutions were implemented and used in varying degrees, with varying effectiveness. The first and most effective solution is the same one as addressed in the above paragraph about failed convergence: providing the code with better initial solutions. By providing the code with a solution set of parameters which is already close to the "best" solution, it's less likely to get stuck in local minima of χ^2 because the code needs to travel a smaller distance in the parameter space. This solution introduces a new problem, however: how to determine a solution set of parameters which is already close to the "best" one.

Because the Milne-Eddington inversion code is fast and efficient at inverting spectra, it's

possible to perform multiple inversions per spectra in a reasonable amount of time. For this reason, for the ME inversions we inverted each spectra five times, starting from different, reasonable, starting parameter sets, and then took the best-fitting inversions. This approach both improved the quality of fits and eliminated the spread of parameters over unreasonable values, meaning it seems to have been an effective solution to the problem.

For the SIR inversion code, the solution to the problem of local minima of χ^2 and non-convergence is a little more difficult, because the more complicated solar model means inversions are more computationally intensive. At first, we tried the same solution with SIR as we did with the ME inversion: inverting each spectra multiple times from reasonable starting parameters. For SIR, solutions are atmospheric models, so for each spectra, we inverted each using 7 initial starting atmospheres. The pre-computed starting atmospheres were example solutions, created by Gafeira et al. [2021]. However, this was far too computationally intensive, even with parallelization and running the code with multiple threads at once.

We found that using pre-computed solutions greatly improved χ^2 and the agreement of inverted parameters between nearby pixels, but that it took far too long to compute if each spectra was inverted many times. If we used only a single initial solution for every spectra, inversions were faster, but χ^2 got worse - additionally, the resulting parameter maps were much more discontinuous and less structured than the we expected. (see the left-most plot in the Fig. 3.4). The fact that adjacent pixels are equally well fit, but parameters between adjacent pixels are not smooth implies that some pixels still getting stuck in local minima of χ^2 . We expect the physical structure of the Sun to be smooth and have no sharp boundaries between adjacent spectra, and if everything goes correctly, so should the inverted parameters. If the inversions get stuck in local minima of χ^2 , they might have equally well fit spectra but have very different inverted parameters.

The solution we developed for this problem is to "shake up" the input initial solutions, to start each inversion from slightly different initial solutions without inverting each spectra many times. By doing this, we hoped to give each spectra more spatially smooth but still realistic solution to start inverting from. The method we developed to do this is to median filter the

output atmospheres of each inversion spatially, and use this median-filtered atmosphere for the next inversion's initial solution. This way, each spectra receives a small "nudge" in parameter space towards the parameters of the surrounding pixels, allowing the inversion to find a more spatially coherent solution for each spectra. This process can even be repeated multiple times, by median filtering the output inverted atmosphere from each round of inversions, and using this as the next initial solution. From our testing, we found that after two rounds of median filtering and re-inputting these as initial solutions, the benefits plateau off, so for all datasets, this process was carried out twice. The resulting inversions improve in not only χ^2 but also in the spatial coherence of the resulting atmospheres, as can be seen visually in the more structured and smooth-looking temperature and χ^2 maps below.

An additional issue which is important to account for is noise - the effect of noise can not be thought of as simply as the local-minima issue, because different realizations of noise might effect the spectra and the resulting inversions in very different ways. To combat this issue, the best possible solution is to invert more spectra, so that a statistical analysis of the distributions of parameters from many spectra will reduce the effect of noise. We used the measured noise level of Hinode's spectropolarimeter for the χ^2 calculations, to look for optimal values of χ^2 ($\chi^2 \approx 1$), and to not overfit the noisy data.

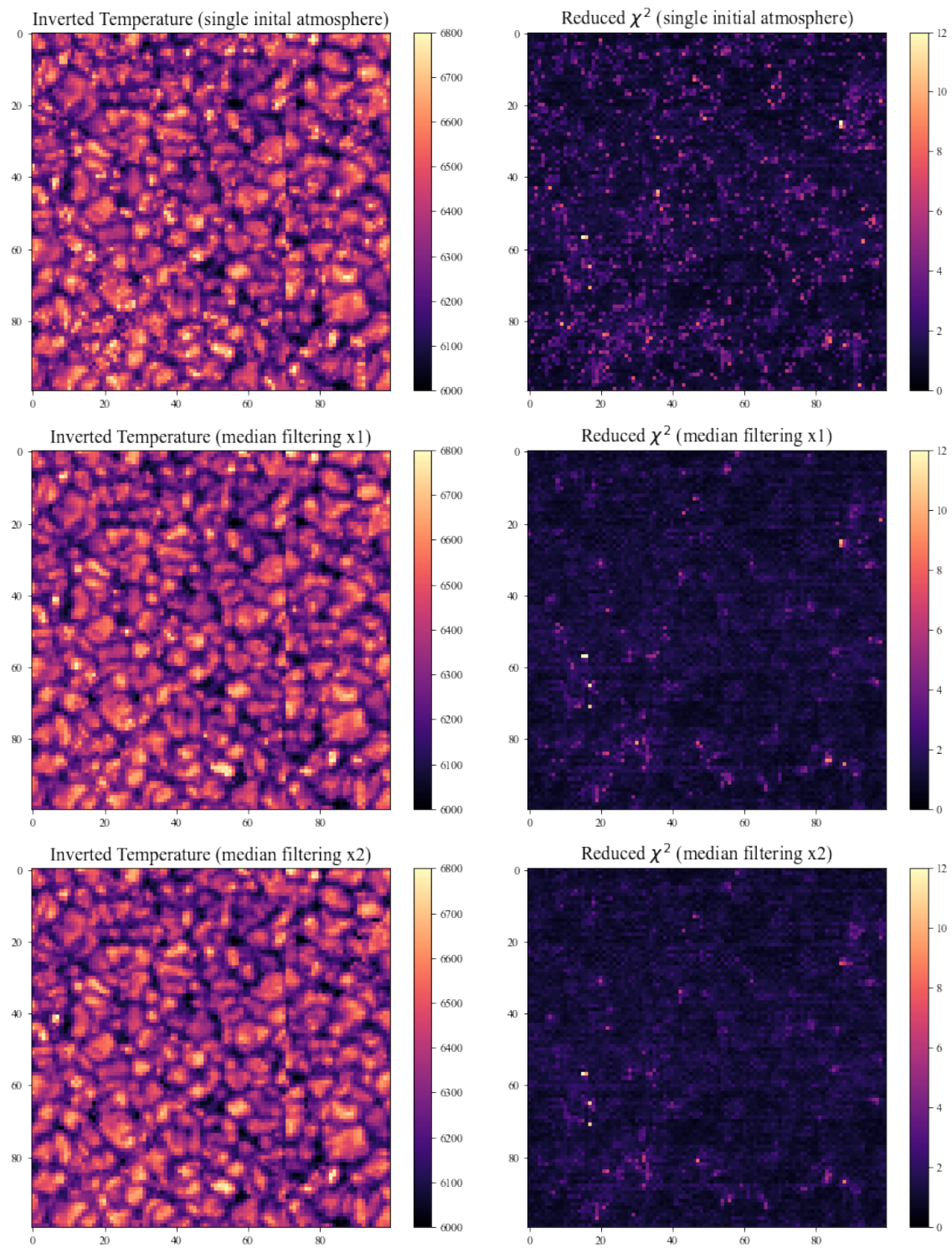


Figure 3.4: Maps of inverted temperatures at $\log \tau = 0$ (right) and calculated χ^2 (left) for increasing rounds of median filtering.

Chapter 4

Analysis

4.1 Filtering & Clustering

In order to characterize the differences in the atmospheric structure between years, it's first useful to separate and partition the data (i.e. pixels), so that the differences between similar parts of the solar photosphere can be more directly compared. In the context of a study of the solar photosphere of the quiet, non-magnetic, Sun, some useful partitions naturally emerge. The first is between magnetic and non-magnetic pixels, so that non-magnetic pixels can be filtered out and we can focus the analysis on the pixels where the variations of the line shapes comes from the changes of the thermodynamic parameters only. Next, we separate the granules and intergranules - this is because we expect granules and intergranules to have different depth stratification of the physical parameters. Additionally, we expect that differences between spectra of a single dataset are much larger than differences in those properties between years. For instance, we expect temperature or velocity structures in granules and intergranules to be significantly different, while differences in averages over the photosphere might change by only a percent or less throughout the solar magnetic cycle. Therefore, it's useful to separate spectra into groups where there are similar physical processes going on - here, granules and intergranules. This means we need a way to reliably separate data into groups, and a way to verify it.

4.1.1 Filtering Pixels with Magnetic Field

Since the data sets are selected with strict requirements to not have any large-scale magnetic elements, the magnetic pixels that are left are typically in smaller patches of weaker magnetic signal, which makes them harder to identify. Being able to reliably separate out non-magnetic pixels from magnetic ones allows us to ensure the pixels left are quiet Sun - however, weak magnetic fields and unresolved magnetic fluxes make this a challenging issue. For the Milne-Eddington Inversion, filtering out magnetic pixels is tricky - this is because the form of the ME model used in this project is the original Milne-Eddington formulation designed for non-magnetic spectral lines, and so it has no way of concluding magnetic fields from inverted spectral lines. This means we needed to determine and test a proxy for the magnetic field strength.

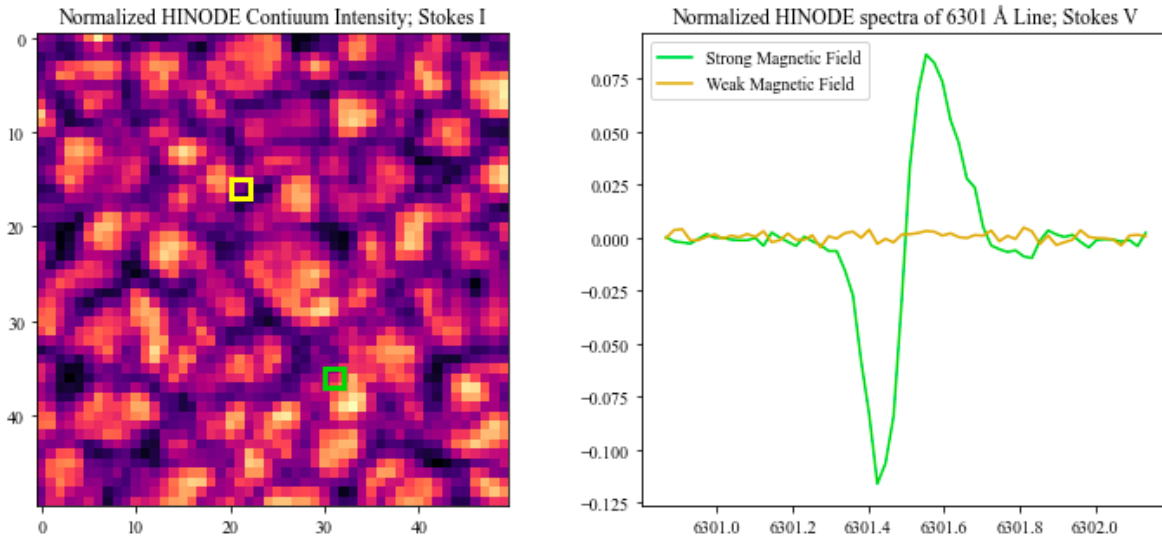


Figure 4.1: The Stokes V spectra of the two boxed pixels.

In practice, it becomes more complicated: the four Stokes components are have both systematic and random noise in them. Since weak magnetic fields produce light with only small differences between polarization states, the signal-to-noise ratio in Stokes Q, U, and V can often be very small. The solution developed for this project is to sum the absolute value of the observed signal over Stokes Q, U, and V, and then set a threshold depending on the relative signal-to-noise

of the data, so that pixels with sufficiently strong magnetic fields can be filtered out and any below that threshold can be left behind:

$$\sum_{\lambda} |Q_{\lambda}| + |U_{\lambda}| + |V_{\lambda}|. \quad (4.1)$$

Once this has been done for every pixel in a dataset, we obtain a map of the magnetic pixels, which can be used in order to exclude pixels where the magnetic field is too strong. The result of this filtering can be seen in the left panel in figure 4.2.

For the SIR inversions, implementing a filter is easier - this is because SIR includes the magnetic field directly in the atmospheric model and infers it from the spectral line polarization. This means that the code includes magnetic field strengths as a free parameter when inverting spectra, and filtering out magnetic pixels is as easy as setting a threshold in magnetic field strength and setting aside any pixels above that threshold. When comparing the two methods, there is strong agreement, meaning that the Polarization Threshold Method is a good proxy for magnetic field strength. For this project, we settled on a magnetic threshold of 250 Gauss, as inverted by SIR. In the spectra that SIR identified to have a magnetic field stronger than 250 Gauss, the polarization threshold method agreed for 90% of them.

4.1.2 K-Means Clustering

In order to partition data into granules and intergranules, a few different methods were tried, before landing on the final solution of K-Means clustering. At first, like the magnetic fields in the Milne-Eddington model, we searched for a proxy of granules or intergranules that is directly measurable, or easily estimated from the observed spectra. The clearest candidate is line-of-sight velocity; we expect granules to be moving upward in the solar atmosphere, since they're hotter and more buoyant, and intergranules to be moving downward. At the center of the solar disk, this corresponds to positive and negative line-of-sight (LOS) velocities respectively, which should be observable by Doppler shifts in atomic line spectra. In practice, however, we quickly learned that a combination of velocity gradients throughout the photosphere and limited spatial resolution of

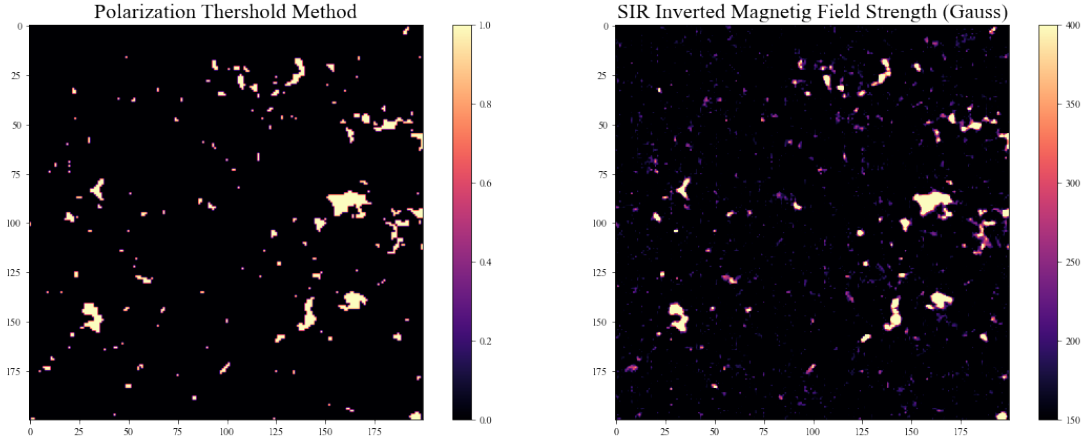


Figure 4.2: Comparing the two methods of filtering magnetic fields: on the left is the polarization threshold method created for the ME model as a proxy for magnetic field strength; on the right is the directly inverted magnetic field from SIR. The color bars have been adjusted to show the similarity of features between the two.

observations mean that using the Doppler shift as a proxy for granules and intergranules does work in some pixels, but not as reliably as desired.

Although using LOS velocities directly was not a reliable enough proxy for granules and intergranules, we still wanted a way to divide these two directly from the spectra, not from inverted parameters; this is because the more directly we can conclude this from observables, the less uncertainty we introduce by subsequent methods or inversions. To do this, we clustered the spectra using K-Means clustering. This is an algorithm for vector clustering developed in 1967 for signal processing by J. Macqueen [1967]. By treating each spectra from the Hinode data as a vector in the wavelength dimension, it's possible to apply K-Means clustering to each dataset, and let the algorithm identify small, sometimes imperceptible similarities between spectra. By configuring the algorithm correctly, K-Means clustering reliably and quickly clusters the data spatially into granules and intergranules. To implement it this project, we used a python version of the algorithm from the scikit-learn [Pedregosa et al., 2011] package. For configuration, we noticed that the pixels which fall in-between granules and intergranules often confuse the code when clustering into only two groups. For this reason, we used three K-Means groups: granules, intergranules, and in-between regions; having an in-between cluster allows for the algorithm to more reliably sort spectra into

granules and intergranules, because it has a cluster for pixels in-between either of the other two groups. Also, physically, we do expect some pixels to fall somewhere between the granules and intergranules as spatially, there is no sharp boundary between the two.

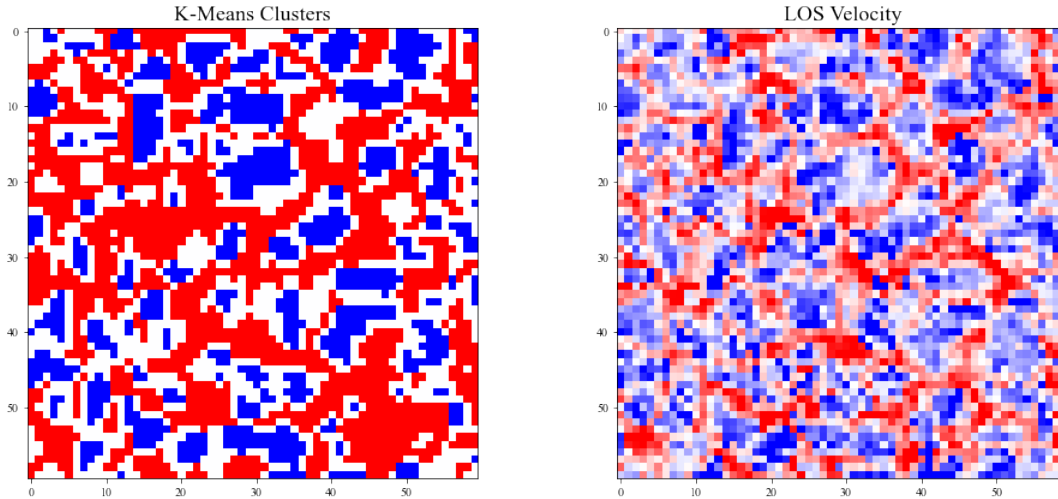


Figure 4.3: Comparing K-Means Clustering and LOS Velocities. K-Means clusters on the left; Inverted LOS velocities on the right. The structures and groupings are similar between both graphs.

To verify the K-Means clustering, we compare the resulting clusters to LOS-velocities. Although, as described above, LOS velocities are not a perfect proxy of granules or intergranules, the two does correspond fairly strongly (Fig. 4.3). By applying K-Means clustering to datasets, it allows us to compare changes in the inverted parameters between granules and intergranules separately over the solar cycle.

4.2 Comparing SIR Inversions to an Independent Inversion Results

With inversions, there's always the lingering question of with what confidence can we conclude inverted parameters as being representative of physical conditions on the Sun. Because of this, carefully analyzing error and scrutinizing the inferred parameters is especially important. With that in mind, we've selected and inverted a dataset that was published in Socas-Navarro [2011] using the NICOLE inversion code [Socas-Navarro et al., 2015], with the goal of comparing if inverted

parameters agree.

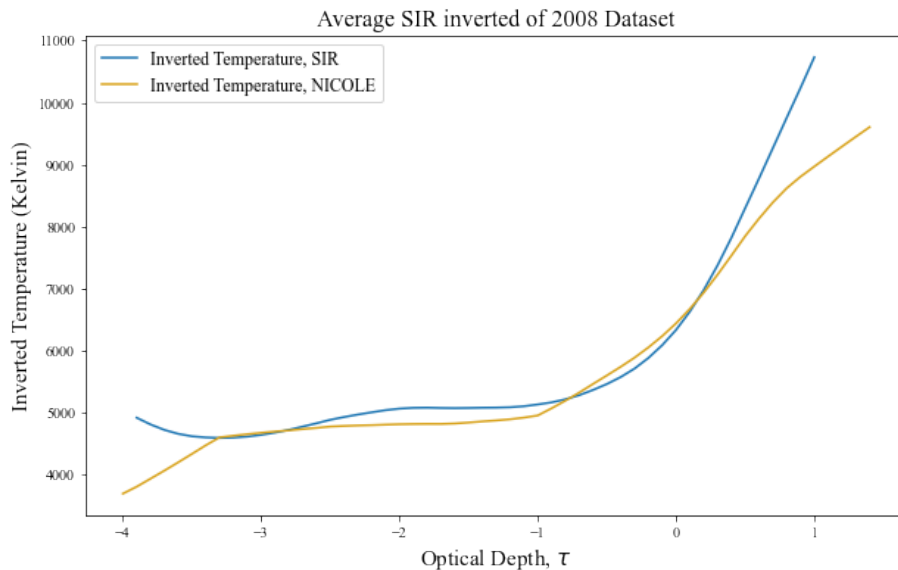


Figure 4.4: Comparing the average temperature between inversion methods. Blue is SIR, yellow is NICOLE inversion of the same dataset.

A few things are important to note about the NICOLE inversion: first, like SIR, NICOLE inverts depth-stratified parameters, but it's clear from the inverted temperature in Fig. 4.4 that the particulars of how the code fits those parameters is different. The way of parametrizing the depth dependence (so called-nodes), is different between the two codes: NICOLE uses linear interpolation while SIR uses higher degree polynomials. The mean temperature stratification is similar in the range where our spectral line is predominantly formed ($\log \tau = 0$ to -2), but the differences still exist. Outside of the line formation region, the differences are more significant.

Despite the general agreement between inverted temperatures of SIR and NICOLE, using this NICOLE inversion to test any of the other properties we focus on for this project, like the temperature gradient, is not as straightforward. Because the two inversion codes disagree by up to a couple hundred Kelvin, the temperature gradients between two depth points can disagree by a few hundred Kelvin. This is an important point on it's own: our measurement of the temperature, as well as other physical parameters, is not only determined by the accuracy and the resolution of

the data, but also by the interpretation method itself. In this case, different inversion codes contain different physics and different numerical solutions and thus yield different inferred values. This is an important caveat to have in mind, and a large-scale research of this kind should double-check all the results using multiple inversion codes, which is a task that has not yet been accomplished, at least not according to the well-known inversion literature.

Chapter 5

Results

For this project, we focus on two quantities in particular to compare between the years: the temperature gradient, and the line-of-sight velocity - although changes in multiple parameters are discussed below. Note that Milne-Eddington and SIR inversion are fundamentally different. First one parametrizes the atmosphere in terms of the analytical expression 2.6, where most of the quantities are depth-independent, while the latter infers depth-dependent temperature, velocity and the magnetic field. Additionally, we are separating the solar surface in two different features: granules and intergranules. Therefore, we will qualitatively compare the quantities that describe the same features, obtained by the same inversion approach, between the two stages of the solar cycle: a minimum (2008) and a maximum (2014).

5.1 Temperature Gradient

The temperature gradient is the difference in photospheric temperatures between two optical depths. In the Milne-Eddington model, the source function gradient, a_1 , is constant in the photosphere. Milne-Eddington source function is related to the temperature, although the conversion is not straightforward and perhaps not even physically meaningful. We still expect the temperature gradient to be loosely related to the source function gradient, allowing us to compare them - at least qualitatively - between inversions. Additionally, using the above method of K-Means clustering, we are able to analyze differences of these parameters between the granules and intergranules. We first analyze the source function gradient, a_1 , from Milne-Eddington inversions. Like mentioned above,

we expect differences in physical structure between the granules and intergranules in a single year to be much larger than the differences in overall structure between years. Due to this, when we compare the distributions of the source function gradient over all spectra, between the two years, the difference is tiny - the differences in means are less than a percent which is too small to conclude that the differences are statistically significant between the years (Fig. 5.1). The distribution is, however, noticeably broader during the solar minimum.

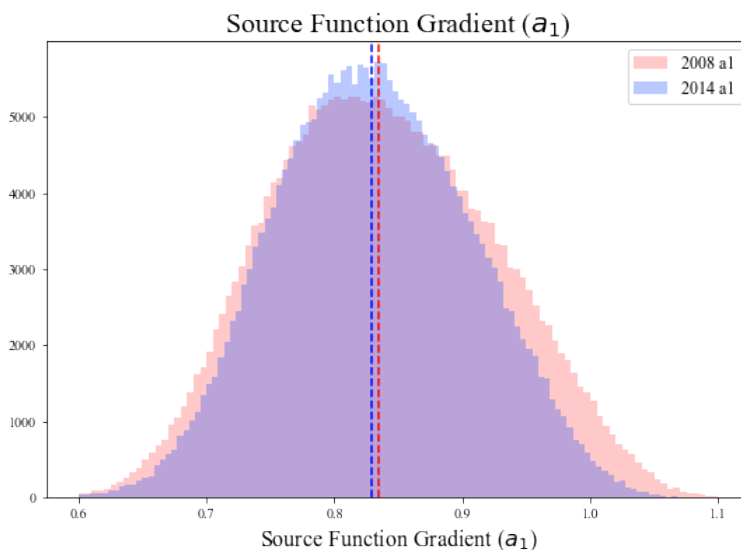


Figure 5.1: Inverted Milne-Eddington Source Function Gradient, of all spectra. Dashed lines denote the mean values of the two distributions.

Next, we've separated the inverted parameters between granules and intergranules, with the distributions shown in Fig. 5.2. What's immediately apparent and interesting is that the small, less than a percent difference mentioned above in the average source function gradient is due almost entirely to the spectra we have classified as the granules. The difference between the mean source function gradient in the granules is 5.5%, while in the intergranules the difference is just a bit more than 1%, but interestingly, in the opposite direction than the granules.

Next, we discuss the temperature gradient from the SIR inversions. This one is a bit more complicated than the source function gradient: in the ME model, the source function is linear

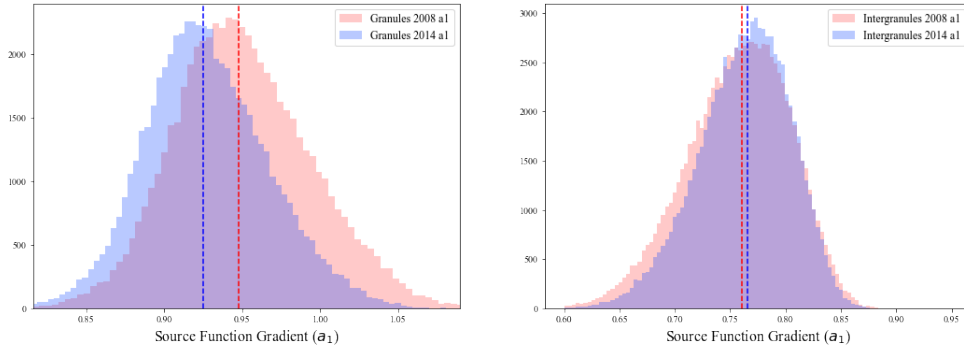


Figure 5.2: Inverted Milne-Eddington source function gradient, in granules (left), and intergranules (right)

and so its gradient had only one value for a given spectrum, independent of height. In the SIR atmosphere, we have a depth-stratified temperature, and so the gradient can be, in principle, defined as a difference between any two depths. For the spectral line we are considering here, the depths where conditions of the photosphere strongly influence the line profile are in the range of $\log(\tau) = 0$ to -2 . We chose to show three different temperature gradients, between paired optical depths (0 and -1), (0 and -2), and finally (-1 and -2).

Below are the gradients in inverted temperatures obtained by applying SIR to the two selected datasets from 2008 and 2014. Although shapes and tail distributions change slightly between optical depths, an important feature of all three graphs is in the differences of distributions between the granules and the intergranules. Like in the Milne-Eddington inversion, we see that the difference in parameters is largely due to the spectra clustered as granules. Additionally, we see that the differences between the two datasets follow a similar trend to the ME inversion: the temperature gradient is similar in the intergranules, but is noticeably higher in 2008 in granules.

In the SIR inversion, the amount of difference depends on the optical depths chosen - between $\log(\tau) = 0$ and -1 , the difference in the means of the temperature gradient is 4.8%. This difference in the means is less for other optical depths, but, interestingly, shows the same patterns in overall distributions: the difference in granules is always larger than in intergranules, and 2008 always has

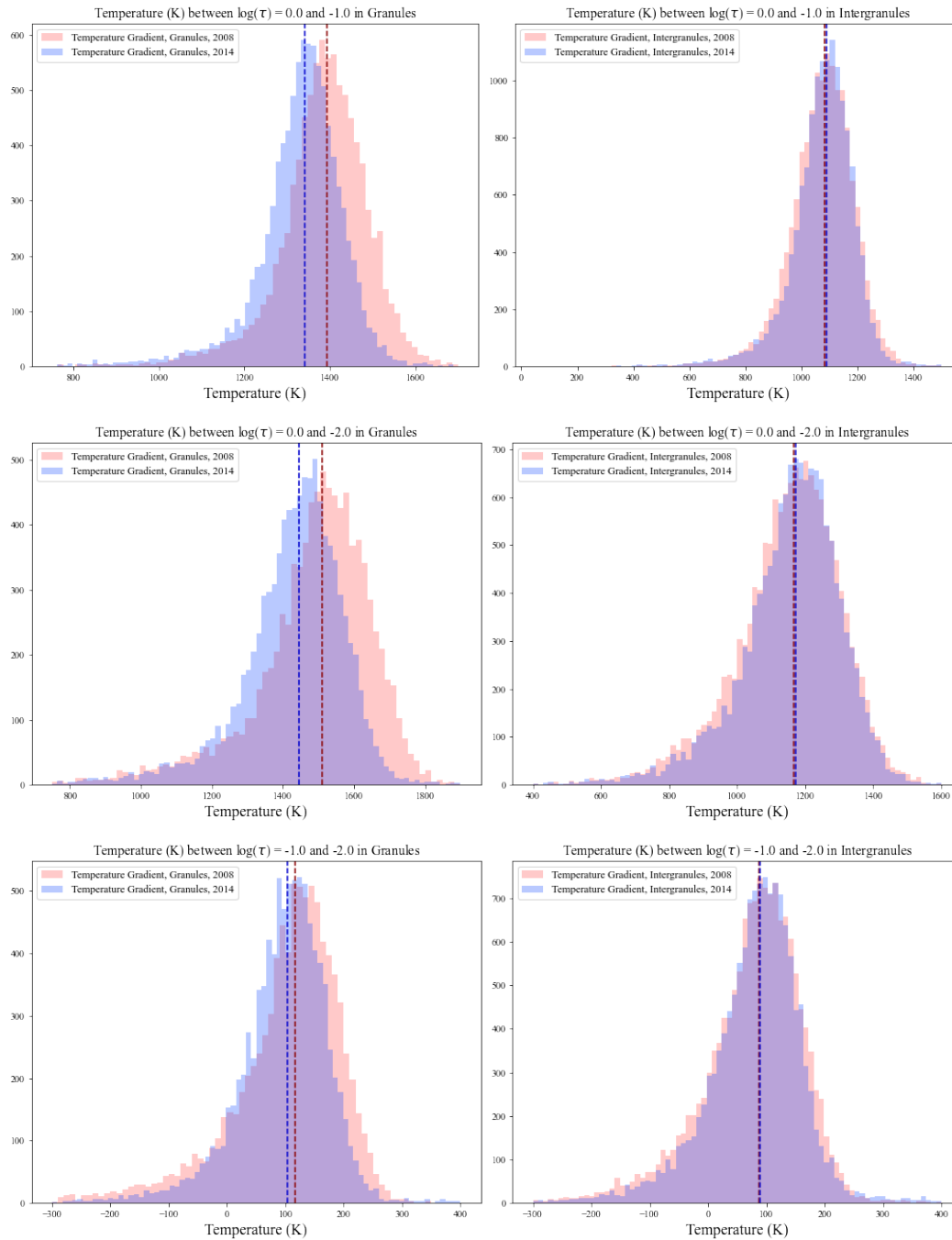


Figure 5.3: Temperature gradient between different pairs of optical depths. From top to bottom, the graphs show temperature gradients between $\log(\tau) = 0$ and -1 ; 0 and -2 ; and -1 and -2 , in granules (left) and intergranules (right).

a higher temperature gradient, regardless of depths chosen (Fig. 5.3).

5.2 Line-of-Sight Velocity

Similar to the case temperature gradients, SIR provides us with height-stratified line-of-sight velocities, while Milne-Eddington estimates some sort of a mean velocity in the line forming region. Because the two are describing related but fundamentally distinct quantities, we again can only compare them qualitatively.

For ME inverted line-of-sight velocity, like in the source function gradient, there is a noticeable difference in the distributions of inverted parameters between granules and intergranules, as seen in Fig. 5.4. In granules, like expected, the mean values are negative, since this corresponds to motion upward in the solar photosphere. Similarly, in intergranules, the mean values are positive. Between years, 2008 shows slightly more extreme line-of-sight velocities, in both granules and intergranules. Finally, differences in means between 2008 and 2014 are a little larger in the granules than in the intergranules.

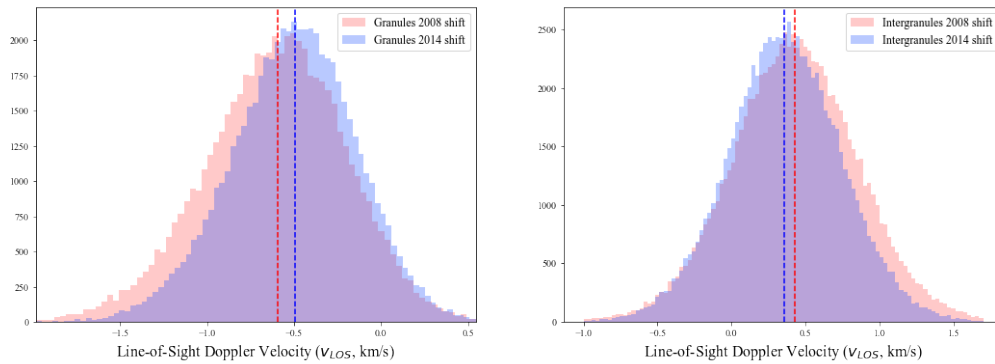


Figure 5.4: Inverted Milne-Eddington Line-of-Sight velocities, in granules (left), and intergranules (right), in km/s.

For line-of-sight velocities inverted from SIR, we compare distributions at optical depths of $\log(\tau) = 0, -1,$ and -2 . These are found in Fig. 5.5. Notably, mean line-of-sight velocities are similar throughout the photosphere between years, but show significant differences in granules at $\log(\tau) = 0$. At this optical depth, the granules have a larger difference in mean line-of-sight velocity, and the difference between the mean line-of-sight velocities of granules and intergranules is larger in 2008.

This agrees qualitatively with the ME inversions.

The qualitative agreement between these two inverted parameters from the Milne-Eddington model and SIR model is significant. For the temperature gradient and the line-of-sight of sight velocity, this is especially true, because of how these parameters are determined. Temperature and source function gradients are determined entirely by the depth of the spectral line. Line-of-sight velocities and velocity gradients are entirely determined by the shift and asymmetry of the spectral line. This means that these two parameters are orthogonal and are determined independent to a large degree. The agreement between ME and SIR inversions of these parameters is therefore not an effect of the inversions or data-processing steps. These are results which independently agree with one another, since they're determined in unique ways which do not influence one another.

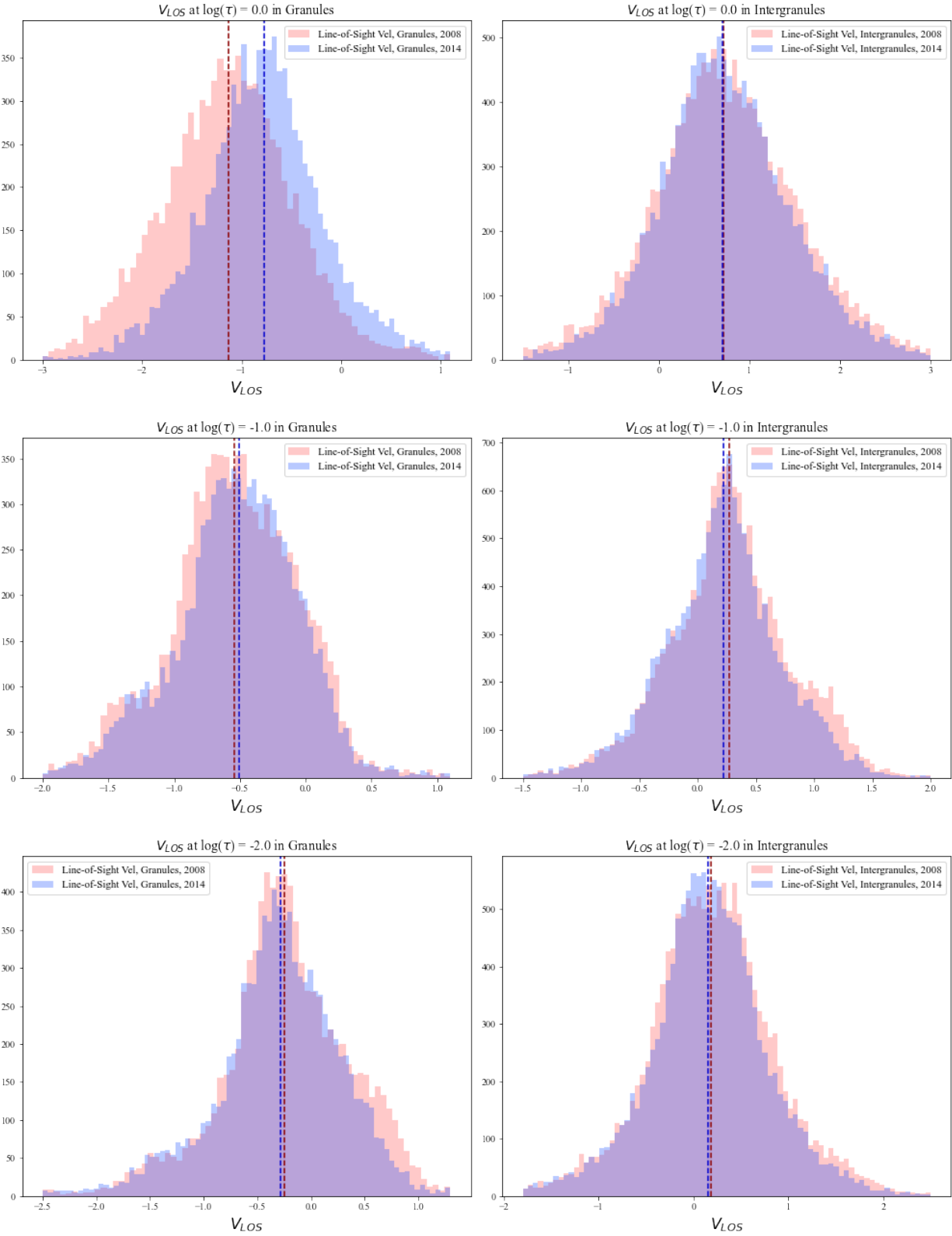


Figure 5.5: Inverted Line-of-Sight velocities by SIR at optical depths of $\log(\tau) = 0, -1,$ and -2 in intergranules (left) and granules (right), in km/s.

Chapter 6

Conclusion

In this project, we search for changes in the photospheric structure of Sun across solar cycle 24 through spectropolarimetric inversions of Hinode data. To do this, we used two inversion codes: a simple Milne-Eddington model and SIR, a more complicated, height-stratified inversion code. By applying both inversion codes to the same datasets, we hope to determine whether a simple Milne-Eddington model was sufficient to find changes in concluded parameters - notably, the source function and temperature gradients, as well as the line-of-sight velocity - and whether the two models agreed qualitatively in these parameters.

From our results (5), it's clear that both the Milne-Eddington and SIR inversions have identified and characterized changes in parameters between a minimum and maximum of the solar-magnetic cycle. Additionally, both inversions agree on the signs and trends of these changes, both between years and between granules and intergranules. Whether or not these results correspond to physical changes in the Sun due to the solar cycle is more difficult to say. This is due to additional sources of uncertainty, like possible instrument degradation from 2008 to 2014 or in the K-Means clustering of the data, as well as limited samples from only the solar minimum and maximum. Because of reasons like these, we can't confirm with certainty that the changes we have found directly correspond to changes in the photosphere. In order to claim this and further confirm these results, inversions of additional datasets from more years throughout the solar cycle as well as independent confirmation from other methods would be required.

Our results imply that the simple model of Milne-Eddington inversions is sufficient in order

to characterize changes of parameters in the quiet Sun, notably the source function gradient and line-of-sight velocity. The Milne-Eddington inversion designed for this project agreed with the more complicated SIR model in distributions and changes these two parameters between quiet-Sun datasets from 2008 and 2014.

6.1 Future Work

Considering that we have seen changes in inverted photospheric parameters, we hope to continue our project in a couple distinct ways. First, we want to invert larger subsections of the selected datasets from 2008 and 2014. With more inverted spectra, we will be able to better characterize the distributions and changes of parameters. Next, we plan to extend this method to more datasets from throughout the solar magnetic cycle. By doing this, we hope to characterize systematic and gradual changes in parameters, not just overall changes between a dataset from the solar minimum and maximum.

Bibliography

- J. M. Borrero, S. Tomczyk, M. Kubo, H. Socas-Navarro, J. Schou, S. Couvidat, and R. Bogart. VFISV: Very Fast Inversion of the Stokes Vector for the Helioseismic and Magnetic Imager. , 273(1):267–293, October 2011. doi: 10.1007/s11207-010-9515-6.
- Subrahmanyan Chandrasekhar. Radiative transfer. 1960.
- Paul Charbonneau. Dynamo Models of the Solar Cycle. Living Reviews in Solar Physics, 7(1):3, September 2010. doi: 10.12942/lrsp-2010-3.
- Frédéric Clette, Leif Svalgaard, José M. Vaquero, and Edward W. Cliver. Revisiting the Sunspot Number. A 400-Year Perspective on the Solar Cycle. , 186(1-4):35–103, December 2014. doi: 10.1007/s11214-014-0074-2.
- II Collins, George W. The fundamentals of stellar astrophysics II. 1989.
- S. Criscuoli, I. Ermolli, H. Uitenbroek, and F. Giorgi. Effects of Unresolved Magnetic Field on Fe I 617.3 and 630.2 nm Line Shapes. , 763(2):144, February 2013. doi: 10.1088/0004-637X/763/2/144.
- Jose Carlos del Toro Iniesta and Basilio Ruiz Cobo. Inversion of the radiative transfer equation for polarized light. Living Reviews in Solar Physics, 13(1):4, November 2016. doi: 10.1007/s41116-016-0005-2.
- R. Gafeira, D. Orozco Suárez, I. Milić, C. Quintero Noda, B. Ruiz Cobo, and H. Uitenbroek. Machine learning initialization to accelerate Stokes profile inversions. , 651:A31, July 2021. doi: 10.1051/0004-6361/201936910.
- B. W. Lites, D. L. Akin, G. Card, T. Cruz, D. W. Duncan, C. G. Edwards, D. F. Elmore, C. Hoffmann, Y. Katsukawa, N. Katz, M. Kubo, K. Ichimoto, T. Shimizu, R. A. Shine, K. V. Streander, A. Suematsu, T. D. Tarbell, A. M. Title, and S. Tsuneta. The Hinode Spectro-Polarimeter. , 283(2):579–599, April 2013. doi: 10.1007/s11207-012-0206-3.
- J. Macqueen. Some methods for classification and analysis of multivariate observations. In In 5-th Berkeley Symposium on Mathematical Statistics and Probability, pages 281–297, 1967.
- D. Orozco Suárez, L. R. Bellot Rubio, and J. C. Del Toro Iniesta. Milne-Eddington inversion of the Fe I line pair at 630 nm. , 518:A3, July 2010. doi: 10.1051/0004-6361/201014374.

- F. Pedregosa, G. Varoquaux, A. Gramfort, V. Michel, B. Thirion, O. Grisel, M. Blondel, P. Prettenhofer, R. Weiss, V. Dubourg, J. Vanderplas, A. Passos, D. Cournapeau, M. Brucher, M. Perrot, and E. Duchesnay. Scikit-learn: Machine learning in Python. Journal of Machine Learning Research, 12:2825–2830, 2011.
- B. Ruiz Cobo and J. C. del Toro Iniesta. Inversion of Stokes Profiles. , 398:375, October 1992. doi: 10.1086/171862.
- Sabrina Sanchez, Alexandre Fournier, and Julien Aubert. The Predictability of Advection-dominated Flux-transport Solar Dynamo Models. , 781(1):8, January 2014. doi: 10.1088/0004-637X/781/1/8.
- Arthur Schuster. Radiation Through a Foggy Atmosphere. , 21:1, January 1905. doi: 10.1086/141186.
- H. Socas-Navarro. A high-resolution three-dimensional model of the solar photosphere derived from Hinode observations. , 529:A37, May 2011. doi: 10.1051/0004-6361/201015805.
- H. Socas-Navarro, J. de la Cruz Rodríguez, A. Asensio Ramos, J. Trujillo Bueno, and B. Ruiz Cobo. An open-source, massively parallel code for non-LTE synthesis and inversion of spectral lines and zeeman-induced stokes profiles. Astronomy & Astrophysics, 577:A7, apr 2015. doi: 10.1051/0004-6361/201424860. URL